Submitted Paper

Applied Spectroscopy
www.s-a-s.org

Applied Spectroscopy
2022, Vol. 76(5) 569–579

DOI: 10.1177/00037028211072583
journals.sagepub.com/home/asp
SAGE

Molecular Emissions from Stretched Excitation Pulse in Nanosecond Phase-Selective Laser-Induced Breakdown Spectroscopy of TiO_2 Nanoaerosols

Gang Xiong[1]*, Yuqian Zhang[1], Christof Schulz[2] and Stephen D. Tse[1]

Abstract

In phase-selective laser-induced breakdown spectroscopy (PS-LIBS), gas-borne nanoparticles are irradiated with laser pulses (~2.4 GW/cm^2) resulting in breakdown of the nanoparticle phase but not the surrounding gas phase. In this work, the effect of excitation laser-pulse duration and energy on the intensity and duration of TiO_2–nanoparticle PS-LIBS emission signal is investigated. Laser pulses from a frequency-doubled neodymium-doped yttrium aluminum garnet (Nd:YAG) laser (532 nm) are stretched from 8 ns (full width at half maximum, FWHM) up to ~30 ns at fixed pulse energy using combinations of two optical cavities. The intensity of the titanium atomic emissions at around 500 nm wavelength increases by ~60%, with the stretched pulse and emissions at around 482 nm, attributed to TiO, enhanced over 10 times. While the atomic emissions rise with the stretched laser pulse and decay around 20 ns after the end of the laser pulse, the TiO emissions reach their peak intensity at about 20 ns later and last longer. At low laser energy (i.e., 1 mJ/pulse, or 80 MW/cm^2), the TiO emissions dominate, but their increase with laser energy is lower compared to the atomic emissions. The origin of the 482 nm emission is explored by examining several different aerosol setups, including Ti–O, Ti–N, and Ti–O–N from a spark particle generator and Ti–O–N–C–H aerosol from flame synthesis. The 482 nm emissions are attributed to electronically excited TiO, likely resulting from the reaction of excited titanium atoms with surrounding oxidizing (carbonaceous and/or radical) species. The effects of pulse length are attributed to the shift of absorption from the initial interaction with the particle to the prolonged interaction with the plasma through inverse bremsstrahlung.

Keywords

Laser-induced breakdown spectroscopy, LIBS, molecular emission, pulse duration, laser-generated plasma, chemiluminescence

Date received: 31 July 2021; accepted: 11 December 2021

Introduction

Laser-induced breakdown spectroscopy (LIBS) has been extensively applied to analyze the composition of almost any type of sample in almost any environment without (or with minimal) sample preparation.[1] In LIBS measurements, the behavior of the laser-generated plasma and the quantitative nature of the emitted signals are influenced by many parameters, such as laser irradiance,[2] laser wavelength,[3,4] matrix and environment,[5] and pulse duration.[6,7] Significant experimental and computational efforts have been devoted to understand better these involved processes to realize accurate, sensitive, and quantitative LIBS measurements and interpretations.[8,9]

The pulse duration of lasers employed in LIBS measurements can range from femtoseconds to nanoseconds, with distinct behaviors resulting in the laser-produced plasma and the optical emissions. Typically, for LIBS with nanosecond lasers, the plasma lasts for over 10 μs; and in the early moments (tens to hundreds of nanoseconds), the plasma emissions are dominated by continuum emissions.[1,10] As the pulse duration in LIBS is shortened to femtoseconds, there are several differences in the laser–matter interaction compared

[1]Department of Mechanical and Aerospace Engineering, Rutgers, The State University of New Jersey, Piscataway, NJ, USA
[2]IVG, Institute for Combustion and Gas Dynamics – Reactive Fluids and CENIDE, Center for Nanointegration Duisburg-Essen, University of Duisburg-Essen, Duisburg, Germany

*Current address: FM Global, Research Division, 1151 Boston-Providence Turnpike, Norwood, MA 02062, USA

Corresponding author:
Stephen D. Tse, Department of Mechanical and Aerospace Engineering, Rutgers, The State University of New Jersey, 98 Brett Road, Piscataway, NJ 08854, USA.
Email: sdytse@rutgers.edu

to that for nanoseconds lasers, such as negligible electron–lattice heating and limited thermal conduction at the short time scale,[11] along with a different mechanism for initial electron generation.[12] The plasma lifetime in femtosecond LIBS (fs-LIBS) is shortened to around 10 μs or even 1 μs,[13,14] and the continuum emission is significantly reduced even in the early phase of plasma formation.[15] Additionally, with plasmas of lower temperature produced by femtosecond pulses, the formation of excited molecules is facilitated.[16–18] In contrast, the longer pulse of conventional nanosecond LIBS reheats the plasma, generally producing higher temperatures,[19] which can dissociate molecules, leaving mainly excited atoms and ions.[20]

The change of pulse duration also affects the LIBS emission intensity. As reported in the literature,[21,22] extending the pulse duration from 20 to 150 ns (with the same pulse energy) by a modified neodymium-doped yttrium aluminum garnet (Nd:YAG) laser leads to approximately two times enhancement in the intensity of atomic emission during the LIBS analysis of bulk liquids and solid surfaces in contact with the liquid.

For all of the LIBS measurements mentioned above, the plasma lifetimes are on the order of 1 μs or longer. However, in recently developed low-intensity phase-selective LIBS (PS-LIBS) using a nanosecond laser,[23] the plasma lifetime is less than 100 ns for nanoaerosol measurements during flame synthesis.[24,25] In this PS-LIBS measurement, the laser irradiance is controlled to be appropriately low (i.e., 2.4 GW/cm^2 or even less with a pulse duration of ~10 ns), to the extent that breakdown only occurs when particles are present but without breakdown of the surrounding gas phase, including the vapor precursor. The absorption–ablation–excitation mechanism in laser–particle interaction of the PS-LIBS process has been scrutinized by comparing the intensities of Rayleigh scattering and atomic emission of aerosol particles at different laser irradiances.[26] The signal from the PS-LIBS measurement can be enhanced by hundreds of times with resonant excitation from the same laser pulse when the laser wavelength is tuned to match a certain atomic transition of a neutral atom or ion.[24,25] The PS-LIBS technique has been successfully applied to conduct two-dimensional measurement of the vapor-to-particle transition process,[27] measuring particle volume fraction at parts-per-billion level,[28] studying sodium release in coal combustion,[29] and examining the doping mechanism during flame synthesis.[30]

For the short-lived plasma in PS-LIBS (~100 ns), it is of fundamental interest to investigate the effect of pulse duration on the plasma properties and the resulting emissions. The laser–matter interaction in laser-induced plasma from solids can be divided roughly into three processes: (i) laser heating and vaporization of the solid, (ii) plasma formation with atomic excitation and ionization in the vapor,[31] and (iii) laser–plasma interaction leading to additional energy deposition through inverse bremsstrahlung. These processes are coupled and can occur almost simultaneously in laser-induced plasma, where the laser energy can be absorbed by the solid or the plasma. By changing the pulse duration, it is possible to modify the temporal overlap and thus how energy is fed into the system. Separating these effects supports the understanding of the emissions caused by laser-induced plasma and thus might lead to further development in laser-based diagnostics by making the most of the related effects.

Phase-selective LIBS can also be a source of potentially interfering signals in laser-induced incandescence (LII) measurements in nanoaerosols,[32] where the aim is to heat the particles to incandescent temperatures without generating additional plasma emission. Depending on the particulate material of the nanoaerosol and the laser fluence, however, there can be a transition and super im position between both processes that must be understood to prevent interference. The transition between both processes can also be used to gain additional information about the particulate material.[33,34] In TiO_2, the transition from LII to LIBS is known to occur at a particularly low threshold, and the combined signal has been termed laser-induced emission (LIE).[35] Altogether, these optical diagnostics methods for nanoaerosols[36,37] provide important input in understanding and designing processes for nanomaterials synthesis.

In this study, the laser pulse is stretched by an optical delay setup to modify the pulse duration in the nanoseconds scale to interact with TiO_2 nanoaerosol for further development and characterization of the PS-LIBS technique. A strong enhancement (~10 times) in a given wavelength range of emissions, later concluded to be TiO molecular emission, is observed. The spectral differences and the temporal behaviors of the Ti-atomic and TiO-molecular emissions under different configurations of pulse stretching are examined.

Experimental Setup

The setup for the spectrally and temporally resolved PS-LIBS measurements is shown in Fig. 1. An Nd:YAG laser (Spectra-Physics Quanta-Ray PRO-250-10) at 10 Hz repetition rate serves as the excitation source, with a pulse duration of about 8 ns at full width at half-maximum (FWHM). The laser beam can be optionally elongated temporally by a pulse stretcher, which consists of two optical ring cavities based on the method described by Kojima and Nguyen,[38,39] thereby adjusting the pulse duration. As the laser beam reaches the beam splitters, 40% of the laser pulse energy gets reflected, while the rest passes into the optical ring cavity. The ring cavity traps and stores a portion of the laser energy, releasing the energy gradually over an extended period, thereby stretching the laser pulse. The beam dumps (BD) in the two cavities can be switched in and out of the light path, yielding four different configurations of the stretcher, that is, with no cavities (BD-1 and BD-2 in light path), with Cavity 2 only (BD-1 in light path, BD-2 out of light path), with Cavity 1 only (BD-1 out of light path, BD-2 in light path), and with both cavities (both BD-1 and BD-2 out of light path). The pulse energy of the input laser beam is fixed for all configurations, and a series of neutral density filters are placed at the outlet of the pulse stretcher to

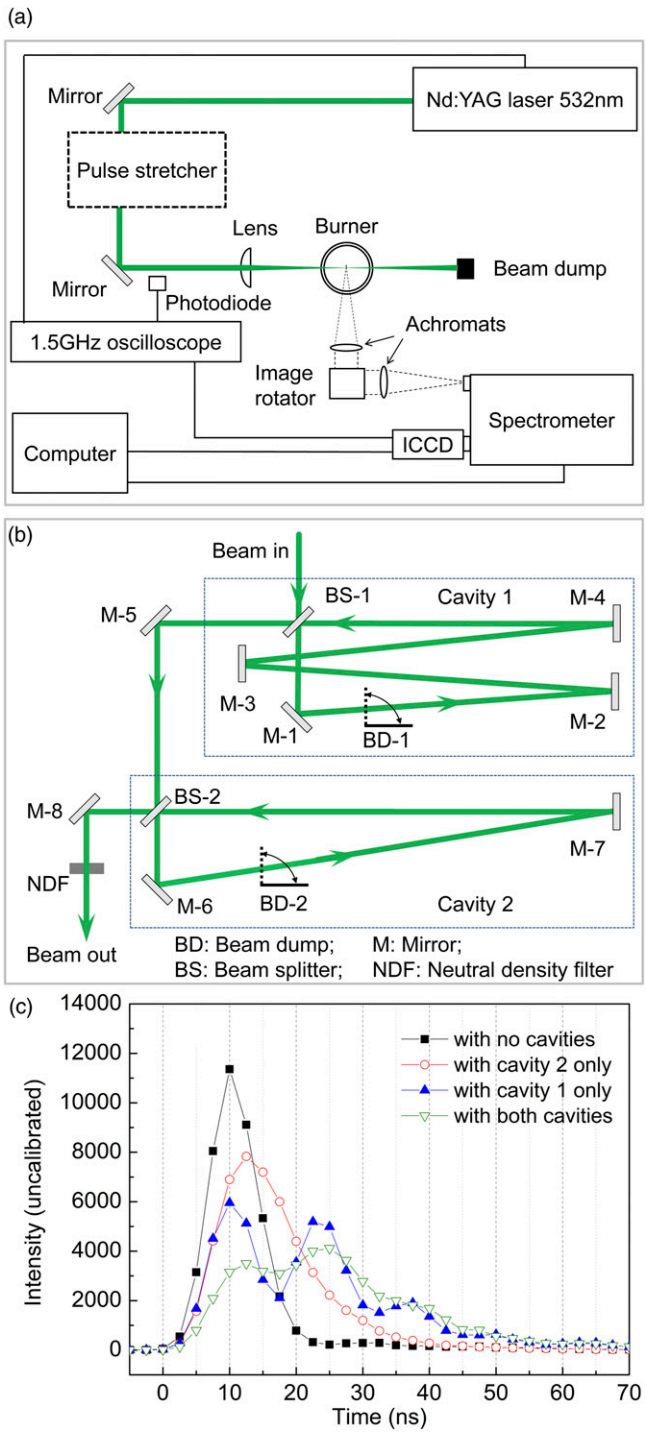

Figure 1. Schematics of (a) the laser diagnostics setup and (b) the pulse stretcher. (c) Plots of the temporal intensity variation of laser pulses under different stretcher configurations as measured by Rayleigh scattering in clean air for nominally identical laser pulse energies of 30 mJ.

adjust the total laser pulse energy to the set value (e.g., 30 mJ/pulse).

The outgoing laser beam from the pulse stretcher is then focused by a 500 mm focal-length, plano-convex fused-silica lens to the region of interest in the flame synthesis flow field, having a beam waist of ~400 μm and a laser fluence of 24 J/cm^2 for a laser pulse energy of 30 mJ/pulse. The emissions are collected at a right angle into a spectrometer (Acton SpectraPro 500i, f = 500 mm, $f\#$ = 5.9, 900 grooves/mm grating, 200 μm entrance slit width) and detected by an intensified charge-coupled device (ICCD) camera (Princeton Instruments PIMAX 3) triggered by the Q-switch output from the laser. The collection optics include two 400 mm focal length achromats (with a diameter of 50.8 mm), an image rotator, and turning mirrors, which project a 1:1 image of the region of interest onto the entrance slit. The collection optics are not UV transparent; therefore, in the detection range relevant in this work, overlap with second-order diffraction of UV signal can be ruled out. The relative timings of Q-switch, laser pulse, and image intensifier gating are monitored with a 1.5 GHz oscilloscope (Agilent Infiniium 54545A). The relative delay time and the gate width of the image intensifier can be adjusted to record the total emission with a wide gate width (e.g., 200 ns) and a fixed delay time (0 ns). Temporal emissions can be deduced from repetitive acquisition using a narrow gate width (e.g., 2.5 ns or 10 ns) with a sequence of delay times, for the steady-state flame synthesis process. Typically, the signal from 300 single laser shots is accumulated on the chip.

The temporal intensity of the laser pulse under different stretcher configurations is characterized by recording Rayleigh scattering from clean air with a gate width of 2.5 ns and a sequence of gate delay times with 2.5 ns interval. Figure 1c shows the temporal intensity variation of the laser pulse for four configurations but with the same total pulse energy of 30 mJ/pulse (measured with an Ophir Nova laser energy monitor after the neutral density filters as shown in Fig. 1b). The unstretched pulses can be fitted with a Gaussian distribution, with a pulse width (FWHM) of 8.4 ns, which is consistent with the specifications of the laser. The pulse width increases to about 14 ns with Cavity 2 only. When using Cavity 1 only (Fig. 1b), the pulse manifests as a series of pulses with an interval of about 14 ns because of the much longer optical delay length (~4.2 m). These individual pulses partially overlap. With both cavities combined, the laser pulse is smoother and lasts for ~30 ns.

To examine the occurrence of Ti and TiO emissions, we use three experimental setups to modify the composition/species in the aerosol and to compare possible routes for TiO* (with the star denoting electronic excitation) formation. Table 1 lists the three experimental configurations. First, a premixed stagnation swirl-flame setup of CH_4, O_2, and N_2 generates TiO_2 nanoparticles, as shown in Fig. S1 (Supplemental Material). The details of the setup can be found in Xiong et al.[24] and Wang et al.[40] Titanium tetra-isopropoxide (TTIP) is carried by N_2 into the flame as the precursor, which decomposes and reacts with other species in the flame to form TiO_2 nanoparticles because of the supersaturation created by the temperature drop from the cooled substrate. The TiO_2 nanoparticles grow in the flow, reaching an average

Table I. Three experimental configurations used in this study.

No.	Name	Purpose	Refs.
1	Stagnation swirl-flame	Main setup, for general study	25, 40
2	Spark particle generator	To create nanoparticles consisting of variable elemental compositions	41
3	Modified Hencken burner	To study the influence of carbonaceous species	44

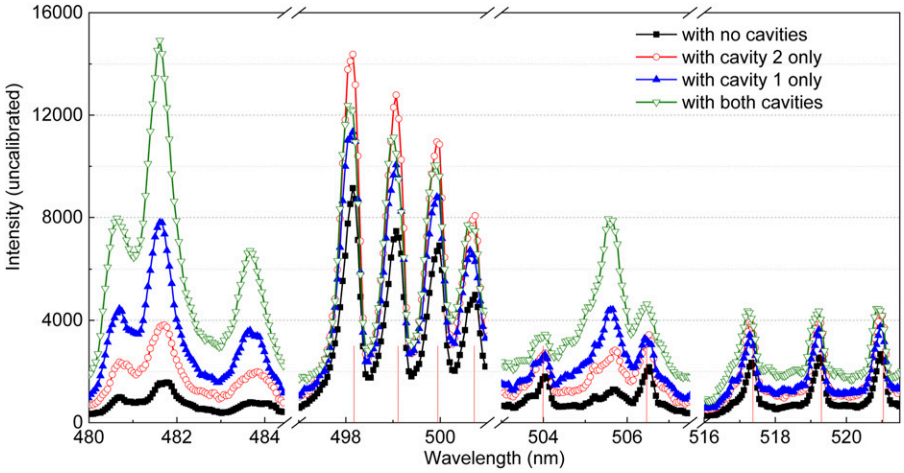

Figure 2. Emission spectra integrated for 200 ns with different stretcher configurations, with the same laser pulse energy of 30 mJ/pulse. Red vertical lines mark the locations of Ti atomic emissions.

size of about 13 nm (with up to 20% variation among particles) before reaching the substrate,[24,40] which is 19 mm downstream from the burner exit. The measurements are carried out along the nozzle centerline axis in the aerosol generated between the nozzle exit and the aluminum cooling plate.

Second, a spark particle generator creates nanoparticles consisting of variable elemental compositions. The spark generator is similar to the one described by Byeon et al.[41] Briefly, there are two titanium rods placed inside a chamber with a gap of ~1 mm between the ends of the rods. During the experiments, a voltage difference of 3 kV is applied to the titanium rods to break down the gas in the gap and ablate Ti (from the electrodes), which then reacts with the environment and forms nanoparticles through homogeneous nucleation in the cooling flow. The environment can be altered between O_2/Ar, N_2, and O_2/N_2 to change the elemental composition of the nanoaerosol.[41–43] PS-LIBS with stretched pulses is conducted at the exit flow of the spark particle generator.

Third, a modified Hencken burner produces nanoparticles in the Ti–O–N–C–H system in non-premixed flames with a tunable C/H ratio to study the influence of carbonaceous species. More details of the modified Hencken burner can be found in Zhang.[44] Briefly, the burner consists of over 200 tubes (with an inner diameter of 0.5 mm) running a 2D array of H_2–O_2/N_2 normal (over-ventilated) diffusion flames to provide uniform temperature and species field downstream, and one central tube (with an inner diameter of 6 mm) for the delivery of TTIP with a carrier gas to generate TiO_2 nanoparticles in the flow field. The flow rates for H_2, O_2, and N_2 are 2, 8, and 6.6 L/min, respectively. The carrier gas is switched between 80% N_2/20 % H_2 and N_2/CH_4, with a total flow rate of 0.5 L/min. The molar fraction of CH_4 in the carrier gas ranges from 9% to 45%. PS-LIBS with a stretched pulse is performed on the aerosol generated from the central diffusion flame, at a location of 2 cm above the exit of the central tube, along the axial centerline.

Results and Discussions

Effect of Laser Pulse Duration

The measurements are first conducted in the stagnation swirl premixed flame setup, at a distance of 14 mm downstream from the burner exit, along the axial centerline, where all TTIP precursors have converted to TiO_2 nanoparticles with a diameter of about 12 nm.[23] Under all stretcher configurations, the breakdown occurs in the PS-LIBS regime, where there are no nitrogen or oxygen atomic emissions (or bremsstrahlung radiation); and the signal is collected almost concurrently with the laser pulse. The gate width of the ICCD is set to 200 ns to collect all the emissions. The emission spectra under different stretcher configurations are shown in Fig. 2, with strong Ti atomic emission lines (i.e., 498.173, 499.107, 499.950, 500.721, 503.996, 506.465, 517.374, 519.297, and 521.038 nm)[45] marked with vertical lines. Without pulse

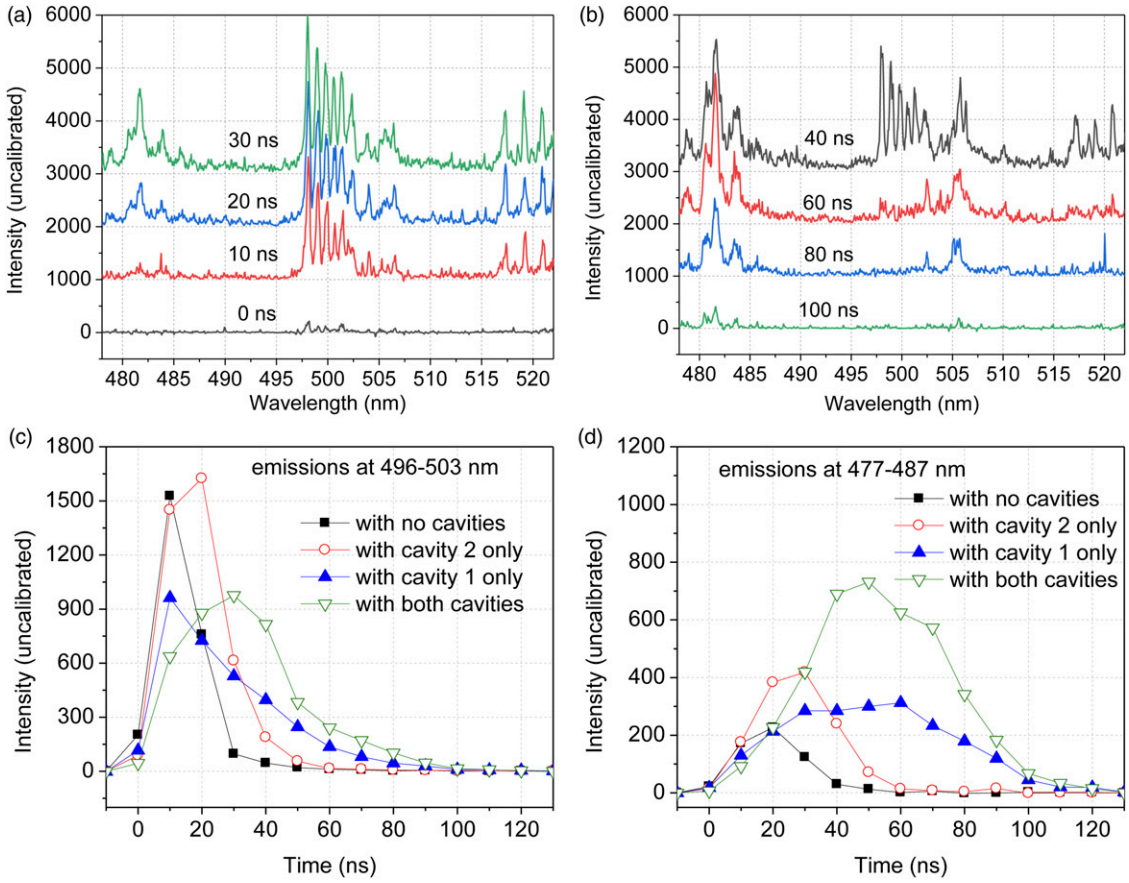

Figure 3. Temporal evolution of emissions with 30 mJ/pulse excitation energy for pulse stretching integrated for 10 ns with different delay times, (a) and (b) emission spectra from 0 to 100 ns with both cavities, (c) and (d) change of emission intensities with different stretching configurations.

stretching, only the titanium atomic emission lines are strong, while the emissions around 482 and 505 nm are fairly weak. However, with pulse stretching, the emissions around 482 and 505 nm are significantly heightened, that is, about 10 times for the emission at 481.666 nm. The Ti atomic emissions around 500 nm are also increased by ~60%, but not as much as the emissions around 482 nm. The emissions around 482 nm can be fitted with three peaks at 480.668, 481.666, and 483.770 nm, while no strong atomic emissions can be found corresponding to the NIST database.[45] Furthermore, how the emission increases with a stretched pulse is different for emissions around 482 nm versus atomic emissions around 500 nm. For the atomic emissions around 500 nm (e.g., 498.173 nm), the signal is boosted by 1.24, 1.58, and 1.35 times with Cavity 1 only, Cavity 2 only, and both cavities, respectively. The highest signal occurs with Cavity 2 only. In contrast, for emissions around 482 nm, the signal is boosted by 2.42, 4.95, and 9.46 times with Cavity 1 only, Cavity 2 only, and both cavities, respectively. The intensities continue increasing as the pulse is stretched further. The emission around 505 nm displays the same trend as does the emission around 482 nm. Besides 482 and 505 nm, emissions around 563 and 595 nm are also significantly augmented in intensity.

The laser-induced plasma excitation temperature is determined by the Boltzmann plot method,[25,31] using the relative intensities of the atomic line emissions around 500 nm (i.e., 498.173, 499.107, 499.950, and 500.721 nm) and 520 nm (i.e., 517.374, 519.297, and 521.038 nm) based on the NIST database.[45] Parameters used in the temperature fitting are listed in Table S1, and the fitted plasma temperatures under different stretcher configurations are shown in Fig. S2 (Supplemental Material). The plasma temperature without the pulse stretcher is determined to be ~7280 K, which decreases to ~6500 K when the laser pulse is stretched with both cavities. However, it should be noted that the plasma temperature fitting assumes partial local thermodynamic equilibrium (LTE) and the absence of signal trapping, for which more work is required to check their validity.[25,46] Moreover, our Boltzmann plot is based on the integrated emission over 200 ns, resulting in a calculated "average" temperature. Although the decrease of temperature leads to the decrease of the instant intensity of the atomic emissions, the total emission

intensity is also related to the temporal evolution of the emissions.

The temporal evolution of the emissions around 482 and 500 nm produced by excitation laser pulse with both cavities is shown in Fig. 3a and b. For the signal detection, the gate width of the camera is set to 10 ns to obtain a sufficient signal with a high signal-to-noise ratio. Note that the time labels in the figure indicate the delay times, for example, label 0 ns denotes that the signal is integrated from 0 to 10 ns after the onset of the laser pulse. The Ti atomic emission around 500 nm rises and reaches the maximum almost simultaneously with the laser pulse (~30 ns) and decays quickly as the laser pulse ends. On the other hand, the emissions around 482 nm peak much later (~50 ns) than do the Ti atomic emissions around 500 nm, but last longer. When the intensities decay to half of their maxima, the durations are ~35, ~50, and ~80 ns for laser pulse, atomic emissions around 500 nm, and emissions around 482 nm, respectively. The observed temporal evolution of the atomic emissions is typical for PS-LIBS measurements of nanoparticle aerosols.[24] However, the temporal emissions around 482 nm are different from the atomic emissions, along with the enhanced emissions around 505.6, 563, and 595 nm. The dissimilar temporal behavior of these enhanced emissions implies a mechanism different than that producing the atomic emissions.

The detailed temporal variation of the emissions with different excitation laser pulse durations using different stretching configurations are further studied, as shown in Fig. 3c and d. To demonstrate the trend, we average the atomic emissions from 496 to 503 nm and from 477 to 487 nm to represent two different emissions. The atomic emissions with different pulse stretchers all follow a similar trend, that is, rising simultaneously with the laser pulse and decaying quickly as the laser pulse ends. The emission at 10 ns with only Cavity 2 is almost the same as that with no cavities, although the laser power at this time is much less. However, at 20 ns, the emission with Cavity 2 is much stronger because of the further excitation of the plasma by the stretched laser pulse. As the laser pulse is stretched more with Cavity 1 or both cavities, the emissions at 10 ns decrease. Nevertheless, the subsequent photons of the pulse keep heating the plasma at 10 ns and thus produce more atomic emissions at 40 ns and later through thermal excitation of the related species.

The temporal evolutions of the emission around 482 nm are markedly different from the atomic emissions around 500 nm under different pulse stretching configurations. Without the pulse stretcher, the emission is weak and decays promptly to zero at around 50 ns, although emitting slightly longer than do the atomic emissions for the same excitation laser pulse duration. With the pulse stretched by Cavity 2 only, the instant emission intensity increases significantly during 20 to 30 ns and decreases to almost zero at 60 ns. With the laser pulse stretched by Cavity 1 only, the emissions continue increasing, albeit moderately, reaching a maximum at 60 ns, with an overall duration of about 100 ns. With the laser

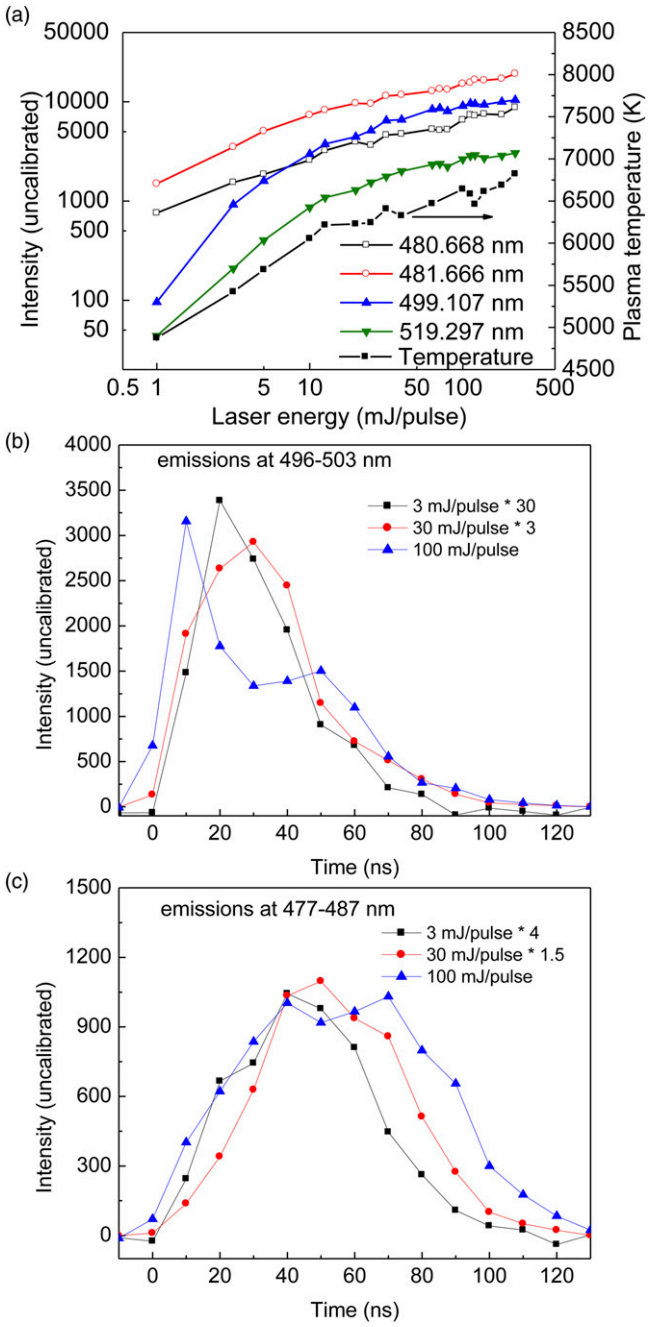

Figure 4. Effect of excitation laser energy, (a) emission intensity and plasma excitation temperature, (b) temporal evolution of emissions at 496–503 nm, and (c) temporal evolution of emissions at 477–487 nm. Both cavities are used for pulse stretching.

pulse stretched by both cavities, the duration of the emissions is about the same as that for Cavity 1 only, but the emission intensity is enhanced prominently by a factor of 2.15. The lifetime of the emissions at 482 nm is closely related to the lifetime of the atomic emissions at 500 nm. As the laser pulse is stretched with Cavity 1 or with both cavities, there are still some atomic emissions at 80 and 90 ns; and the 482 nm emission decays quickly to zero after the plasma is gone. This

result indicates that the presence of the plasma, although weak at 90 ns, influences the strong emissions around 482 nm. Such influence could be from the plasma itself or the high characteristic temperature, which is discussed later.

Dependence of Emission on Laser Energy and Location in the Flow Field

The excitation laser energy (and thus the produced plasma intensity) is then varied to investigate the dependence of the 482 nm emission and atomic emission on the excitation laser energy. For this purpose, the laser pulse is stretched by both cavities, and a series of absorptive neutral density filters (Edmund Optics #63-470, with optical densities from 0.1 to 2.5) are utilized to modify the laser pulse energies. The intensities of two typical atomic lines at 499.107 and 519.297 nm, and two emission peaks around 482 nm (i.e., 480.668 and 481.666 nm), versus a series of laser excitation energies from 1 to 220 mJ/pulse, are plotted in Fig. 4a. Typical emission spectra at three laser energies, that is, 1, 3, and 30 mJ/pulse, are shown in Fig. S3 (Supplemental Material). The emissions all increase as the laser energy increases; however, the trend is different between the atomic lines and the emission around 482 nm, especially for the low laser energies from 1 to 10 mJ/pulse. For the atomic lines at 499.107 and 519.297 nm, the intensities increase quickly at the beginning (1–10 mJ/pulse), and then the increasing rate decreases. However, for the emissions at 480.668 and 481.666 nm, the intensities keep increasing moderately. These emissions around 482 nm are less affected by the low intensity of the plasma, as compared to the atomic emissions around 500 and 520 nm. The plasma temperatures are also fitted by the Boltzmann plot method,[25,31] and are shown as a function of laser pulse energy in Fig. 4a. The temperatures are 4880, 5420, 5684, and 6055 K for cases with laser energies of 1, 3, 5, and 10 mJ/pulse, respectively.

When the laser energies increase, the temporal evolution of the emissions changes as well, as shown in Fig. 4b and c. Note that the intensities are multiplied by appropriate factors for a better comparison, as indicated in the figure. For the atomic emissions around 500 nm, as shown in Fig. 4b, the temporal evolution between 3 and 30 mJ/pulse is close, with one peak intensity at 20–30 ns. As the laser energy increases to 100 mJ/pulse, there are two peak intensities, at 10 and 50 ns, respectively. However, for all laser energies, the atomic emissions decay after 50 ns. For the emissions around 482 nm, the decay time is delayed at higher laser energies.

Phase-selective LIBS with a stretched pulse (with both cavities) is applied to the swirl premixed flame burner at different distances downstream from the exit of the burner to study the effect of the growing size of the particles along the flow-field axis.[24] The emission spectra along different distances are shown in Fig. 5. At a distance of 6 mm away from the burner exit, the particle size is ~5 nm,[24] and there are no

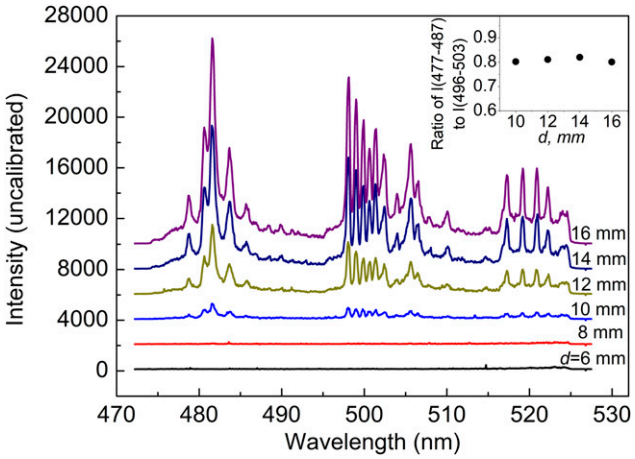

Figure 5. Emission spectra measured along the axis of the swirl burner. The inset shows the ratio of the integrated emission intensity of 477–487 nm to the intensity of 496–503 nm.

emissions. As the nanoparticles grow in the flame-synthesis flow field, increasing their size and volume fraction,[24] the intensities of the emissions increase, which indicates that the phase selectivity is maintained with a stretched excitation pulse. The intensities of emissions around 482 and 500 nm rise with increasing distance from the burner exit along the axis; however, interestingly, the emission intensity ratio of 477–487 nm to 496–503 nm remains constant, as plotted in the inset. Along the axis, the size of the particles increases, but the elemental composition remains the same. The constant ratio of the two emissions may be related to the elemental composition of the nanoparticles in the sampling volume.

Exploration of the Origin of the Enhanced Emission

Further investigations are conducted to decipher the origin of the significantly enhanced emissions. A linear polarizer is placed in front of the image rotator (Fig. 1) to check the emissions' polarization by rotating the line polarizer's direction. Figure S4 (Supplemental Material) shows s-polarized and p-polarized emissions around 482 and 607 nm. As expected, the N_2 Raman at ~607 nm (2331 cm^{-1} shift with 532 nm laser excitation) is s-polarized. However, the emission at ~482 nm shows similar intensity for both s-polarized and p-polarized components, which signifies that the emission at ~482 nm is not polarized. The result distinguishes it from polarized emissions (such as Raman and laser-induced fluorescence) and emphasizes that the excitation here is purely thermal.

The emissions around 482, 563, and 590 nm match several transition bands in the TiO C3Δ–X3Δ transitions well.[47,48] For example, the emission around 482 nm could be attributed to the (4,2), (3,1), and (2,0) bands in the C3Δ–X3Δ transition system. The radiative lifetime of the excited TiO species in the C3Δ state is determined experimentally to be around 30 ns.[49,50] The TiO molecules could be excited by plasma[51] or

chemical reaction of Ti atoms with surrounding gaseous species.[47,52,53] The laser-induced plasma produces Ti atoms that can react readily with gaseous species to produce excited TiO*, with corresponding chemiluminescent emission. Moreover, plasma-excited Ti atoms (a^5F) require no activation energy to react with oxygen-containing species such as O_2, NO, and N_2O to form TiO*,[54] leading to reaction rates two orders of magnitude higher than those of ground-state Ti (a^3F).[55,56] Because of the different mechanisms leading to emission, the intensity changes of the emissions around 482 and 500 nm with respect to laser energy are expected to be different, as shown in Fig. 4.

To assess whether the TiO emission may be caused by direct plasma excitation of TiO species, we conduct PS-LIBS measurements with stretched pulses in another setup making aerosols of TiO_2 nanoparticles. Titania nanoparticles are produced by a spark generator with titanium rods as electrodes and O_2/Ar or O_2/N_2 as flowing gas.[43,44] Three kinds of flowing gases, including O_2/Ar, N_2, and O_2/N_2, are employed to generate Ti–O, Ti–N, and Ti–O–N species. Yet, under all these conditions, no enhanced emissions are observed around 482 nm. As TiO exists in the laser-induced plasma in the Ti–O and Ti–O–N system, the absence of emissions around 482 nm implies that the emission at ~482 nm is not from the plasma excitation of TiO. These results also imply that the TiO emissions are not from the reaction of Ti with species in the Ti–O–N system. It should be noted that the TiO chemiluminescence emission spectra also depend on the electronic state of the Ti atom (e.g., ground a^3F state or excited state such as a^5F) and the gaseous oxidant (e.g., N_2, N_2O, or O_2).[54,57,58] For example, as shown in Dubois and Gole,[47] the chemiluminescence spectra from the Ti–O_2, Ti–NO_2, and Ti–N_2O reactions are very different in terms of the relative intensities at different wavelengths. The results lead to the assumption that the TiO emission observed in our experiments is chemiluminescence resulting from *reactions* in the Ti–O–N–C–H system.

Further experiments are conducted on the Ti–O–N–C–H system using a diffusion-flame-based Hencken-type burner, where the carrier gas composition in the center tube is switched between N_2/H_2 and N_2/CH_4 to change the concentration of carbonaceous species. The emission spectra with different carrier gases are shown in Fig. 6, with the intensities normalized to the peak at 498.173 nm. With N_2/H_2 as a carrier gas to deliver TTIP to the hot flow field, emissions around 482 nm can be observed, with a maximum value of 0.25. When the carrier gas switches from N_2/H_2 to N_2/CH_4 (91% N_2 and 9% CH_4 to keep the same flame height), the emission around 482 nm significantly increases. As the concentration of CH_4 increases from 9 to 45%, there is only a slight increase in the emission around 482 nm.

There are significantly higher concentrations of carbonaceous species and radical species in hydrocarbon flames than those in hydrogen flames.[59] As revealed in Senba et al.,[58], the reaction rate of Ti with some carbonaceous species could be

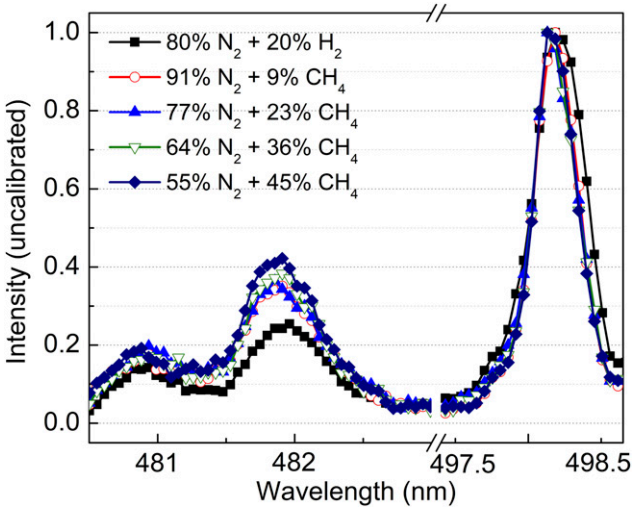

Figure 6. Emission with different gas environments above the Hencken-like burner, with 30 mJ/pulse excitation energy and both cavities for pulse stretching.

orders of magnitude higher than other species. It is likely that carbonaceous species or radical species in the flame, such as CO_2, CO, and OH, react with excited Ti atoms resulting in TiO* chemiluminescence. A hypothesis about the effect of pulse duration in this study is then proposed based on the above reasoning. With a short pulse (no pulse stretcher), TiO_2 nanoparticles vaporize, and plasma is formed in the close vicinity of the nanoparticle. However, because of the rapid cooling following the plasma expansion, there is not enough time in the high-temperature region to facilitate the reaction and production of TiO*. Longer (stretched) pulses can continue to feed energy into the plasma to sustain a sufficiently high temperature condition (but not too high where decomposition of radicals/molecules outcompetes their formation); and with the right reactive species from the flame, the observed TiO* chemiluminescence emission is engendered. Nevertheless, more evidence is needed, and the detailed kinetics require further study.

Conclusion

A nanosecond laser pulse is optically stretched to investigate the effects of pulse duration on the nanosecond-plasma produced during phase-selective LIBS (PS-LIBS) of gas-borne titania nanoparticles. With the stretched pulse, there is a significant enhancement of emissions around 482 nm (attributed to TiO molecular emissions) compared to the mild enhancement of the Ti atomic emissions around 500 nm. The temporal evolution of the emission with the stretched laser pulse shows that the emissions around 482 nm rise later than do the atomic emissions but last longer. The 482 nm molecular emission dominates at low laser pulse energy, and its intensity is less dependent on the laser pulse energy than are the 500 nm atomic emissions. Aerosol systems with different

elemental compositions are used to investigate the origin of the molecular emission. The results suggest that the 482 nm emission is chemiluminescence from excited TiO species from the reaction of excited Ti with oxygen-containing species. A prolonged interaction between the laser pulse and plasma could be facilitated with a longer pulse, sustaining a longer high-temperature condition for chemical reactions to produce excited TiO species and chemiluminescence. These results demonstrate that in the nanosecond-plasma, the duration of the nanosecond laser pulse not only affects the atomic emissions but also plays an important role for the molecular emissions.

The enhanced emissions also imply the potential development of double-pulse PS-LIBS, which may carry the advantages of phase-selectivity and enhanced emission from double pulse conventional LIBS. Moreover, the results demonstrate that excited species and the reactions in the plasma can be strongly affected by the pulse duration, along with the temporal variation in laser fluence. Therefore, by changing the pulse duration and temporal fluence profile, it may be possible to change the plasma temporal evolution and the associated chemical reactions.[60]

Acknowledgments

The authors would like to thank Drs Thomas Dreier and Jan Menser at the University of Duisburg-Essen for their insightful discussions and Professor Jeong Hoon Byeon at Yeungnam University for help with the spark particle generator.

Declaration of Conflicting Interests

The author(s) declared no potential conflicts of interest with respect to the research, authorship, and/or publication of this article.

Funding

The author(s) disclosed receipt of the following financial support for the research, authorship, and/or publication of this article: This work was supported by the Army Research Office through grant W911NF-17-1-0111 and by the Mercator Fellowship at the University of Duisburg (German Research Foundation project number 262219004) for S. Tse.

ORCID iD

Stephen D. Tse https://orcid.org/0000-0003-4380-4853

Supplemental Material

All supplemental material mentioned in the text is available in the online version of the journal.

References

1. D.A. Cremers, L.J. Radziemski. Handbook of Laser-Induced Breakdown Spectroscopy. Hoboken, New Jersey: John Wiley and Sons, 2013. 2nd ed.
2. R.E. Russo, X. Mao, H. Liu, et al. "Laser Ablation in Analytical Chemistry: A Review". Talanta. 2002. 57(3): 425-451.
3. Q. Ma, V. Motto-Ros, F. Laye, et al. "Ultraviolet versus Infrared: Effects of Ablation Laser Wavelength on the Expansion of Laser-Induced Plasma into One-Atmosphere Argon Gas". J. Appl. Phys. 2012. 111(5): 053301.
4. L. St-Onge, V. Detalle, M. Sabsabi. "Enhanced Laser-Induced Breakdown Spectroscopy Using the Combination of Fourth-Harmonic and Fundamental Nd:YAG Laser Pulses". Spectrochim. Acta, Part B. 2002. 57(1): 121-135.
5. R. Noll. Laser-Induced Breakdown Spectroscopy: Fundamentals and Applications. Berlin: Springer, 2014.
6. A. Bogaerts, Z. Chen. "Effect of Laser Parameters on Laser Ablation and Laser-Induced Plasma Formation: A Numerical Modeling Investigation". Spectrochim. Acta, Part B. 2005. 60(9): 1280-1307.
7. X. Zeng, X.L. Mao, R. Greif, R.E. Russo. "Experimental Investigation of Ablation Efficiency and Plasma Expansion During Femtosecond and Nanosecond Laser Ablation of Silicon". Appl. Phys. A. 2005. 80(2): 237-241.
8. D.W. Hahn, N. Omenetto. "Laser-Induced Breakdown Spectroscopy (LIBS), Part II: Review of Instrumental and Methodological Approaches to Material Analysis and Applications to Different Fields". Appl. Spectrosc. 2012. 66(4): 347-419.
9. F.J. Fortes, J. Moros, P. Lucena, et al. "Laser-Induced Breakdown Spectroscopy". Anal. Chem. 2013. 85(2): 640-669.
10. A.W. Miziolek, V. Palleschi, I. Schechter. Laser-Induced Breakdown Spectroscopy (LIBS): Fundamentals and Applications. Cambridge: Cambridge University Press, 2006.
11. B.N. Chichkov, C. Momma, S. Nolte, et al. "Femtosecond, Picosecond and Nanosecond Laser Ablation of Solids". Appl. Phys. A: Mater. Sci. Process. 1996. 63(2): 109.
12. D. Du, X. Liu, G. Korn, et al. "Laser-Induced Breakdown by Impact Ionization in SiO_2 with Pulse Widths from 7 ns to 150 Fs". Appl. Phys. Lett. 1994. 64(23): 3071.
13. J.R. Freeman, S.S. Harilal, P.K. Diwakar, et al. "Comparison of Optical Emission from Nanosecond and Femtosecond Laser Produced Plasma in Atmosphere and Vacuum Conditions". Spectrochim. Acta, Part B. 2013. 87: 43-50.
14. V. Piñon, D. Anglos. "Optical Emission Studies of Plasma Induced by Single and Double Femtosecond Laser Pulses". Spectrochim. Acta, Part B. 2009. 64(10): 950-960.
15. B. Le Drogoff, J. Margot, M. Chaker, et al. "Temporal Characterization of Femtosecond Laser Pulses Induced Plasma for Spectrochemical Analysis of Aluminum Alloys". Spectrochim. Acta, Part B. 2001. 56(6): 987-1002.
16. J. Serrano, J. Moros, J.J. Laserna. "Molecular Signatures in Femtosecond Laser-Induced Organic Plasmas: Comparison with Nanosecond Laser Ablation". Phys. Chem. Chem. Phys. 2016. 18(4): 2398-2408.
17. Q. Wang, A. Chen, W. Xu, et al. "Effect of Lens Focusing Distance on AlO Molecular Emission from Femtosecond Laser-Induced Aluminum Plasma in Air". Opt. Laser Technol. 2020. 122: 105862.
18. Q. Wang, A. Chen, H. Qi, et al. "Influence of Distance between Sample Surface and Geometrical Focal Point on CN Emission

Intensity from Femtosecond Laser-Induced PMMA Plasmas". Phys. Plasmas. 2019. 26(7): 073302.
19. D. Zhang, A. Chen, Q. Wang, et al. "Influence of Target Temperature on H Alpha Line of Laser-Induced Silicon Plasma in Air". Phys. Plasmas. 2018. 25(8): 083305.
20. X. Bai, V. Motto-Ros, W. Lei, et al. "Experimental Determination of the Temperature Range of AlO Molecular Emission in Laser-Induced Aluminum Plasma in Air". Spectrochim. Acta, Part B. 2014. 99: 193-200.
21. B. Thornton, T. Sakka, T. Masamura, et al. "Long-Duration Nano-Second Single Pulse Lasers for Observation of Spectra from Bulk Liquids at High Hydrostatic Pressures". Spectrochim. Acta, Part B. 2014. 97: 7-12.
22. T. Sakka, H. Oguchi, S. Masai, et al. "Use of a Long-Duration Ns Pulse for Efficient Emission of Spectral Lines from the Laser Ablation Plume in Water". Appl. Phys. Lett. 2006. 88(6): 061120.
23. Y. Zhang, G. Xiong, S. Li, et al. "Novel Low-Intensity Phase-Selective Laser-Induced Breakdown Spectroscopy of TiO_2 Nanoparticle Aerosols During Flame Synthesis". Combust. Flame. 2013. 160(3): 725-733.
24. G. Xiong, S. Li, Y. Zhang, et al. "Phase-Selective Laser-Induced Breakdown Spectroscopy of Metal-Oxide Nanoparticle Aerosols with Secondary Resonant Excitation during Flame Synthesis". J. Anal. At. Spectrom. 2016. 31(2): 482-491.
25. G. Xiong, S. Li, S.D. Tse. "Tuning Excitation Laser Wavelength for Secondary Resonance in Low-Intensity Phase-Selective Laser-Induced Breakdown Spectroscopy for In-Situ Analytical Measurement of Nanoaerosols". Spectrochim. Acta, Part B. 2018. 140: 13-21.
26. Y. Ren, S. Li, Y. Zhang, et al. "Absorption-Ablation-Excitation Mechanism of Laser-Cluster Interactions in a Nanoaerosol System". Phys. Rev. Lett. 2015. 114(9): 093401.
27. Y. Zhang, S. Li, Y. Ren, et al. "Two-Dimensional Imaging of Gas-to-Particle Transition in Flames by Laser-Induced Nanoplasmas". Appl. Phys. Lett. 2014. 104(2): 023115.
28. Y. Zhang, S. Li, Y. Ren, et al. "A New Diagnostic for Volume Fraction Measurement of Metal-Oxide Nanoparticles in Flames Using Phase-Selective Laser-Induced Breakdown Spectroscopy". Proc. Combust. Inst. 2015. 35(3): 3681-3688.
29. Y. Yuan, S. Li, Q. Yao. "Dynamic Behavior of Sodium Release from Pulverized Coal Combustion by Phase-Selective Laser-Induced Breakdown Spectroscopy". Proc. Combust. Inst. 2015. 35(2): 2339-2346.
30. Y. Ren, Y. Zhang, S. Li, C.K. Law. "Doping Mechanism of Vanadia/Titania Nanoparticles in Flame Synthesis by a Novel Optical Spectroscopy Technique". Proc. Combust. Inst. 2015. 35(2): 2283-2289.
31. S. Amoruso, R. Bruzzese, N. Spinelli, R. Velotta. "Characterization of Laser-Ablation Plasmas". J. Phys. B: At. Mol. Opt. Phys. 1999. 32(14): R131.
32. H.A. Michelsen, C. Schulz, G.J. Smallwood, S. Will. "Laser-Induced Incandescence: Particulate Diagnostics for Combustion, Atmospheric, and Industrial Applications". Prog. Energy Combust. Sci. 2015. 51: 2-48.
33. J. Menser, K. Daun, T. Dreier, C. Schulz. "Laser-Induced Atomic Emission of Silicon Nanoparticles During Laser-Induced Heating". Appl. Opt. 2017. 56(11): E50-E57.
34. J. Menser, K. Daun, C. Schulz. "Interrogating Gas-Borne Nanoparticles Using Laser-Based Diagnostics and Bayesian Data Fusion". J. Phys. Chem. C. 2021. 125(15): 8382-8390.
35. S. Maffi, F. Cignoli, C. Bellomunno, et al. "Spectral Effects in Laser Induced Incandescence Application to Flame-Made Titania Nanoparticles". Spectrochim. Acta, Part B. 2008. 63(2): 202-209.
36. T. Dreier, C. Schulz. "Laser-Based Diagnostics in the Gas-Phase Synthesis of Inorganic Nanoparticles". Powder Technol. 2016. 287: 226-238.
37. T.A. Sipkens, J. Menser, T. Dreier, et al. "Laser-Induced Incandescence for Non-Soot Nanoparticles: Recent Trends and Current Questions". Appl. Phys. B. 2021. (in review).
38. J. Kojima, Q.-V. Nguyen. "Laser Pulse-Stretching with Multiple Optical Ring Cavities". Appl. Opt. 2002. 41(30): 6360-6370.
39. J. Kojima, Q.-V. Nguyen. "Spontaneous Raman Scattering Diagnostics: Applications in Practical Combustion Systems". In: M. Lackner, F. Winter, A.K. Agarwal, editors. Handbook of Combustion. Weinheim, Germany: Wiley-VCH, 2010. Part 2, Chap. 5, Pp. 125-154.
40. J. Wang, S. Li, W. Yan, et al. "Synthesis of TiO_2 Nanoparticles by Premixed Stagnation Swirl Flames". Proc. Combust. Inst. 2011. 33(2): 1925-1932.
41. J.H. Byeon, J.H. Park, J. Hwang. "Spark Generation of Monometallic and Bimetallic Aerosol Nanoparticles". J. Aerosol Sci. 2008. 39(10): 888-896.
42. J.-T. Kim, J.-S. Chang. "Generation of Metal Oxide Aerosol Particles by a Pulsed Spark Discharge Technique". J. Electrost. 2005. 63(6): 911–916.
43. H.C. Oh, J.H. Ji, J.H. Jung, S.S. Kim. "Synthesis of Titania Nanoparticles via Spark Discharge Method Using Air as a Carrier". Mater. Sci. Forum. 2007. 544–545: 143-146.
44. Y. Zhang. Flame Synthesis of Tungsten-Doped Titanium Dioxide Nanoparticles. [M.S. Thesis]. New Brunswick, NJ: Rutgers University, 2016.
45. A. Kramida, Y. Ralchenko, J. Reader, et al. "NIST Atomic Spectra Database (Ver. 5.9)". National Institute of Standards and Technology. https://www.nist.gov/pml/atomic-spectra-database [accessed Dec 20 2020].
46. G. Cristoforetti, A. De Giacomo, M. Dell'Aglio, et al. "Local Thermodynamic Equilibrium in Laser-Induced Breakdown Spectroscopy: Beyond the McWhirter Criterion". Spectrochim. Acta, Part B. 2010. 65(1): 86-95.
47. L.H. Dubois, J.L. Gole. "Bimolecular, Single Collision Reaction of Ground and Metastable Excited States of Titanium with O_2, NO_2, and N_2O: Confirmation of D00(TiO)". J. Chem. Phys. 1977. 66(2): 779-790.
48. J.G. Phillips. "Molecular Constants of the TiO Molecule". Astrophys. J., Suppl. Ser. 1973. 26: 313-331.
49. J. Feinberg, S.P. Davis. "Lifetime Measurement in the α System ($C3\Delta3$-$X3\Delta3$) of TiO". J. Mol. Spectrosc. 1978. 69(3): 445-449.

50. R.E. Steele, C. Linton. "Flame Spectroscopy of TiO: Radiative Lifetimes and Oscillator Strengths of the α (C3Δ-X3Δ) System". J. Mol. Spectrosc. 1978. 69(1): 66-70.
51. C.G. Parigger. "Atomic and Molecular Emissions in Laser-Induced Breakdown Spectroscopy". Spectrochim. Acta, Part B. 2013. 79: 4-16.
52. K. Honma, Y. Tanaka. "Excited State Reaction Dynamics of Ti (A5FJ)+ O_2→ TiO (A3Φ, B3Π, C3Δ)+ O Studied by a Crossed-Beam Velocity Map Imaging Technique". J. Chem. Phys. 2015. 142(15): 154307.
53. R. Yamashiro, Y. Matsumoto, K. Honma. "Excited State Reaction Dynamics of Ti(AF5J)+O2→TiO(A,B)+O Studied by a Crossed-Beam Technique". J. Chem. Phys. 2009. 131(4): 044316.
54. R. Vetter, C. Naulin, M. Costes. "Oxidation Reactions of Ti(a_3F_J, a_5F_J) Atoms with O_2, NO and N_2O by Crossed Beams". Phys. Chem. Chem. Phys. 2000. 2(4): 643-649.
55. D.E. Clemmer, K. Honma, I. Koyano. "Kinetics of Excited-State Titanium (A5F) Depletion by Nitric Oxide, Oxygen, Nitrous Oxide, and Nitrogen". J. Phys. Chem. 1993. 97(44): 11480-11488.
56. D. Ritter, J.C. Weisshaar. "Kinetics of Neutral Transition-Metal Atoms in the Gas Phase: Oxidation of Titanium (A3F) by Nitric Oxide, Oxygen, and Nitrous Oxide". J. Phys. Chem. 1989. 93(4): 1576-1581.
57. C. Linton, H.P. Broida. "Flame Spectroscopy of TiO: Chem-iluminescence". J. Mol. Spectrosc. 1977. 64(3): 382-388.
58. K. Senba, R. Matsui, K. Honma. "Kinetics of Depletion of Ti (A3F), Ti (A5F), V (A4F), and V (A6D) Atoms by Simple Hydrocarbons". J. Phys. Chem. 1995. 99(38): 13992-13999.
59. G.P. Smith, D.M. Golden, M. Frenklach, et al. "GRI-Mech 3.0". 2011. http://www.me.berkeley.edu/gri_mech [accessed Dec 20 2021].
60. A. Casavola, A. De Giacomo, M. Dell'Aglio, et al. "Experimental Investigation and Modelling of Double Pulse Laser Induced Plasma Spectroscopy Under Water". Spectrochim. Acta, Part B. 2005. 60(7): 975-985.

DOI: 10.1177/00037028211072583
URN: urn:nbn:de:hbz:465-20230825-123225-5